Design & Control of Bearingless drive for Rim Driven Thruster

Wouter MANENSCHIJN[a], Niels KUIPERS, Bauke KALMA

a Insubmo BV, Anne Wadmanwei 4a, 8914BD Leeuwarden, Netherlands, wouter@insumo.nl

Abstract

A motor design and control strategy for a bearingless rim-driven thruster is proposed that obviates the need for a conventional radial bearing, greatly reducing mechanical complexity and wear. The modelling of the system is explained along with the conrol strategy, including a cascaded control scheme. The physical implementation in a working prototype with combined windings is presented and test results are reveiled. These display the functioning of the bearingless drive at various rotational speeds. The results are discussed and future research directions are identified.

Keywords: Bearingless drive, Active Magnetic Bearing, Hub-less Rim-driven thruster

1. Introduction

Hub-less rim-driven thrusters (see figure 1) are a novel type of electric ship propulsion units with numerous advantages. Due to the open propeller configuration organic debris and hazardous materials, like ropes and plastics, can easily find their way through without getting entangled. When designed well, they are also extremely silent, resulting in a very low acoustic and magnetic signature. The open propeller is the only moving part within the thruster, therefore wear of mechanical parts is minimized. However, a good and robust rotor bearing system is needed and this directly designates the main challenge. This paper focuses on the integrated electromagnetic bearing, also known as bearingless drive. Together with a water-lubricated thrust bearing it is part of a uniquely designed hybrid-bearing system. Applying this frictionless hybrid bearing system reduces losses and improves the machines overall efficiency. Furthermore, removing the need for oil as lubricant removes any pollution risks. The novelty of the dual purpose electric rim-drive does ask for a thorough motor design and control strategy, which will be elaborated on in the next sections. First, existing literature will be considered. Then, the motor design and control strategy will be presented, along with the physical implementation in a working prototype. Lastly, results are presented and discussed.

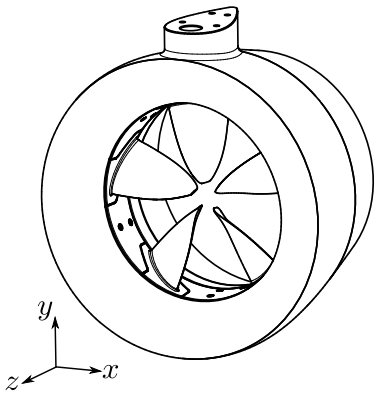

Figure 1: Hub-less rim-driven thruster (Insumo B.V.)

2. Prior Art

Magnetic levitation has been studied for many years, as it provides frictionless rotation with minimal energy dissipation. Furthermore, it has many applications in precise positioning equipment. Regular Active Magnetic Bearings (AMB) generally require a relatively large amount of space, leading to the need for a longer shaft (Chen et al. 2019). Considering the application of a rim-driven thruster, this is highly detrimental. Hence the bearingless drive comes to mind. Bearingless drives have been studied for several different applications, including medical pumps and mixers (Wang et al. 2019). They are an ideal bearing solution for slice drives, as they require minimal space in the axial direction. So far, most bearingless drives are relatively low in power, i.e. less than 30kW (Chen et al. 2019). Furthermore, existing bearingless drives most often apply separate windings to generate the levitating forces. Combined windings have been researched only recently and few industrial applications are known (Sokolov et al. 2021). Another challange for the application of the rim-driven thruster is the fact that the entire machine is submerged during operation. Active magnetic bearings have been applied before in such conditions (Ahad & Ahmad 2021), however a seperate motor is used for the driving torque. What is proposed in this work is, unlike prior art, a bearingless drive using combined windings, applicable for high power rim-driven thrusters that operate in underwater conditions.

3. Design & Modeling

In this paper we will assume that the translations along the z-axis (see figure 1) and rotations around the y and x axes are restrained by the water-lubricated axial bearings. These are the subject of another study, but will be taken for granted here. What remains are translations along x and y, and rotation around z. In order to control these degrees of freedom, the permanent magnet (PM) motor, inrunner design, is electrically split in three equally spaced stator segments. Each segment or motor having a mechanical angle of 120 degrees compared to the next, therefore denoted by subscript 0, 120 and 240. Each segment then is able to provide a torque to the rotor, as well as a radial force on the rotor, as depicted in figure 2.

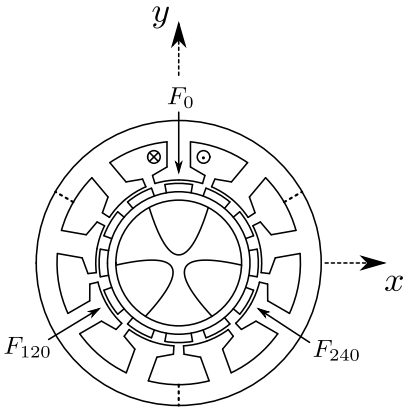

Figure 2: Schematic view of the PM-motor

Now that the motor has been split into three parts, each separate motor remains a three phase machine, resulting in a total of 9 phases. These can be transformed using the Park and Clarke transforms to the dq-reference frame. Overall, we thus need to control six currents: three d-currents that result in forces on the rotor and three q-currents that produce torques. The torques can simply be added as a scalar, while the forces can be added as vectors, resulting in a resultant force on the rotor. Taking into account the negative stiffness of the rotor relative to the stator, we can maintain the rotor in the centre of the stator. Considering the mechanical domain, we can derive the following set of equations:

$$\begin{bmatrix} \dot{x} \\ \ddot{x} \\ \dot{y} \\ \ddot{y} \\ \dot{\theta} \\ \ddot{\theta} \end{bmatrix} = \begin{bmatrix} 0 & 1 & 0 & 0 & 0 & 0 \\ \frac{c_x}{m} & 0 & 0 & 0 & 0 & 0 \\ 0 & 0 & 0 & 1 & 0 & 0 \\ 0 & 0 & \frac{c_y}{m} & 0 & 0 & 0 \\ 0 & 0 & 0 & 0 & 0 & 1 \\ 0 & 0 & 0 & 0 & 0 & p_{prop} \end{bmatrix} \cdot \begin{bmatrix} x \\ \dot{x} \\ y \\ \dot{y} \\ \theta \\ \dot{\theta} \end{bmatrix} + \begin{bmatrix} 0 & 0 & 0 \\ \frac{1}{m} & 0 & 0 \\ 0 & 0 & 0 \\ 0 & \frac{1}{m} & 0 \\ 0 & 0 & 0 \\ 0 & 0 & \frac{1}{J_{zz}} \end{bmatrix} \cdot \begin{bmatrix} F_x \\ F_y \\ T \end{bmatrix} \tag{1}$$

where x denotes the position in x-direction, y the position in y-direction. θ the angular position, c the magnetic stiffness between rotor and stator, m the rotor mass, p_{prop} the rotor frictional losses, J_{zz} the rotor inertia, F_x the input force in x direction, F_y the input force in y direction and T the driving torque on the rotor. Taking into account the geometry of the machine, the input forces and torques are related to the motor currents as follows:

$$\begin{bmatrix} F_x \\ F_y \\ T \end{bmatrix} = \begin{bmatrix} 0 & -\frac{1}{2}\sqrt{3}K_F & \frac{1}{2}\sqrt{3}K_F & 0 & 0 & 0 \\ K_F & -\frac{1}{2}K_F & -\frac{1}{2}K_F & 0 & 0 & 0 \\ 0 & 0 & 0 & K_T & K_T & K_T \end{bmatrix} \cdot \begin{bmatrix} i_{d_0} \\ i_{d_{120}} \\ i_{d_{240}} \\ i_{q_0} \\ i_{q_{120}} \\ i_{q_{240}} \end{bmatrix} \tag{2}$$

where K_F is the current-to-force factor which is assumed equal and constant for each motor segment, K_T the current-to-torque factor, also equal and constant for each motor, i_{d0} the current on the d-axis for motor 0, up to $i_{q_{120}}$, the current on the q-axis for motor 240. Equation 2 is a simplification assuming that the d and q currents are completely separate and do not interfere. Furthermore, in practice, the factor from current to force and torque will depend on the x,y position of the rotor. However, as deviations in x and y are small, this simplification seems justified.

Using equations (1) and (2) we can see the relation between currents and positions. However, the motor input are voltages. Modeling each phase as an RL-circuit, the relation between the input voltages and the resulting currents can be described in the d-q reference frame as follows:

$$\dot{i_{d_0}} = -\frac{R_{d_0}}{L_{d_0}} \cdot i_{d_0} + \frac{1}{L_{d_0}} \cdot U_{d_0} \tag{3}$$

The equations for the d and q currents of the other motor segments are identical to equation (3) and can be written in compact form as:

$$\dot{\vec{i}} = \frac{R}{L} \cdot \vec{i} + \frac{1}{L} \cdot \vec{U} \tag{4}$$

with $\vec{i}\ (6 \times 1)$ containing the six currents and $\vec{U}\ (6 \times 1)$ the six voltages. Combining these equations with equations 1 and 2 results in the description of the system as a whole.

4. Control Strategy

In order to control the machine as a whole, the electrical and mechanical domain are considerd seperately. First, a quick current controller is designed, which is then combined in a cascaded control loop with a controller for the mass-spring system as well as the rotational speed controller. Schematically, the overall control scheme is depicted in figure 3. Note that the speed control and the q-currents are omitted here for simplicity's sake, as this part of the dynamics is considerably slower than the position dynamics. However, one can imagine that a similar control loop is used with the q rather than the d currents and the speed instead of the position.

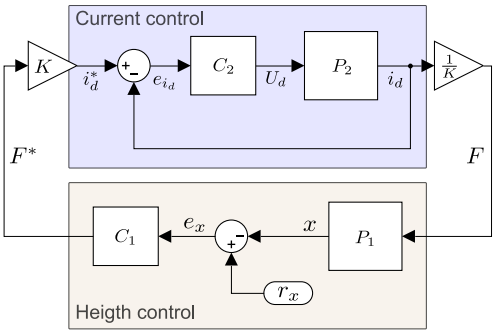

Figure 3: Schematic control overview

4.1 Current Control

Generally, controlling a current in an RL-circuit is relatively straight-forward and has been applied many times before. To this end, a classic PI-controller is used. The gain and integration constant are chosen based on the inductance and resistance of the coils. By design, the resistance and inductance on both the d and q axes are equal for each motor segment. Hence the same controller can be re-used. This PI-current control results in a settling time of roughly 0.5ms.

4.2 Height control

The most challanging part of the control scheme is the position (height) control. As the rotor is highly magnetic, it has a large negative stiffness, forcing it away from the operating point. This force has to be compensated very rapidly to remain in control. A PID-controller is designed with adequate gains to overcome this negative stiffness and keep the rotor in place. Figure 4 shows how the controller moves the unstable poles to the left-half of the complex plane, thus stabilizing the system. Note that the values on the imaginary axis are of the order 10^{-6}, meaning oscillations are almost completely ruled out.

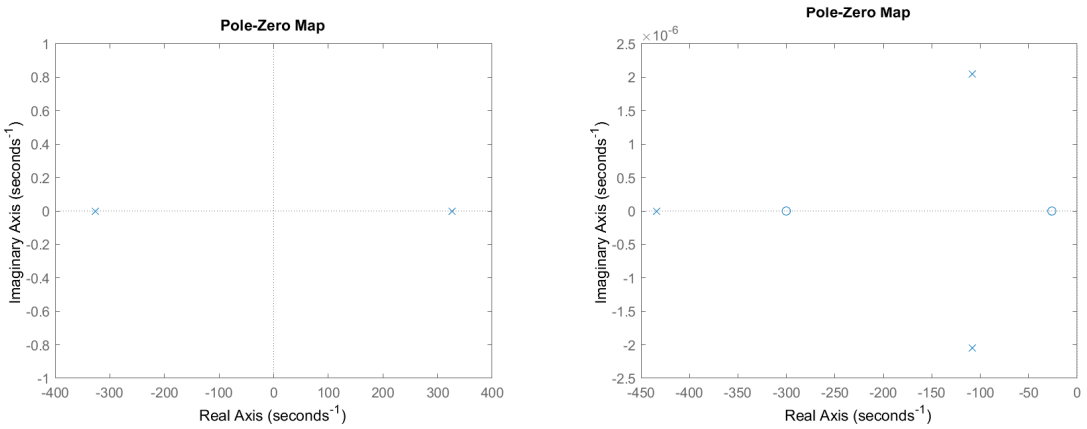

(a) Open loop poles *(b) Closed loop poles*

Figure 4: Movement of unstable poles by applying PID height-control

5. Implementation

As a prototype, a 4kW version of the rim-driven thruster is build with 12 permanent magnet pole pairs and 18 coils. For this proof of concept, the coils are connected in series and powered by a 60V power supply. Pulse Width Modulation is applied to supply the desired voltages. The power electronics are connected to a d-SPACE setup combined with MATLAB/Simulink to allow quick and accurate signal processing. The system operates at 16kHz and parameters can be adjusted real-time. Voltages, currents, x,y positions and angle are measured and used as control signals. Later the angular measurement is replaced with an observer, such that the encoder can be removed. The most important system parameters are summarized in table 1.

Stiffness	**Mass**	**Current to force factor**	**Inductance**	**Resistance**	**Peak Flux**	**Nr of windings**
c	m	K_f	L	R	$\hat{\Phi}$	n
-426000	4	5	$176e^{-6}$	$27.5e^{-3}$	$4.05e^{-4}$	28
$[N/m]$	$[kg]$	$[N/A]$	$[H]$	$[\Omega]$	$[Wb]$	[-]

Table 1: System parameters for a 4 kW prototype

Figure 5 shows the control setup connected to the latest prototype, which is a $20kW$ version of the rim-driven thruster. Testing of this larger machine is still ongoing and results will be available in due time.

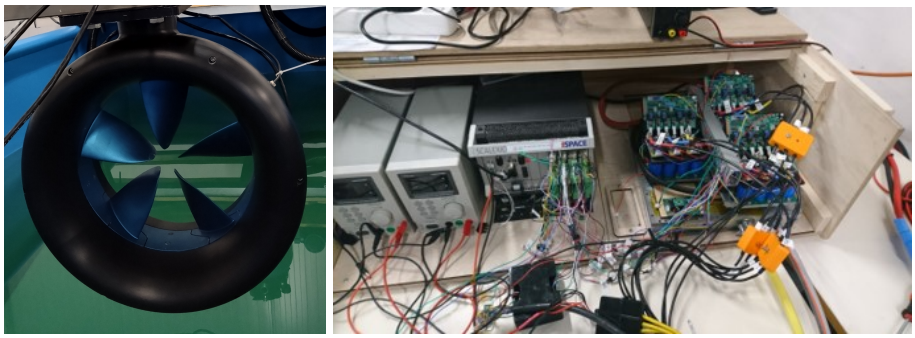

Figure 5: 20 kW hubless rim-driven thruster and control setup

6. Results

Applying the proposed control strategy to the real machine allowed levitation of the rotor through its entire rpm range (0-1300 rpm). Figure 6 shows the orbit plots of the rotor at increasing rotational speeds. It can be observed that the movement around the equilibrium point increases slightly with an increase in rotational speed. Overall though, the distance from the origin does not grow beyond 0.1 mm, which is an acceptable deviation. The nominal gap from rotor to stator is 1mm, so there is no risk of physical contact. Figure 7 shows the corresponding d-currents of a single motor segment. As the deviations around the equilibrium point increase, the required currents to compensate for this movement also increase. Higher rotational speeds are not presented here, because the in-house test-rig does not contain a sufficient volume of water to use the machine's full power. However, the same machine has been used in the field as well. Here, attached to a vessel, the motor has been operated at full power without problems.

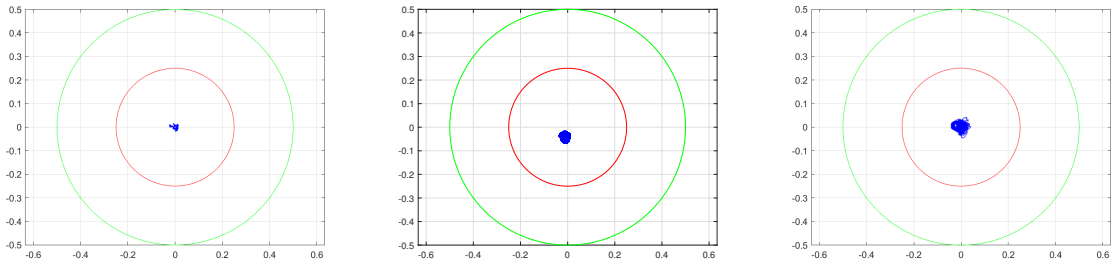

(a) 120 rpm *(b) 360 rpm* *(c) 480 rpm*

Figure 6: Orbit plots at various rotational speeds. (x and y axes represent displacement in [mm])

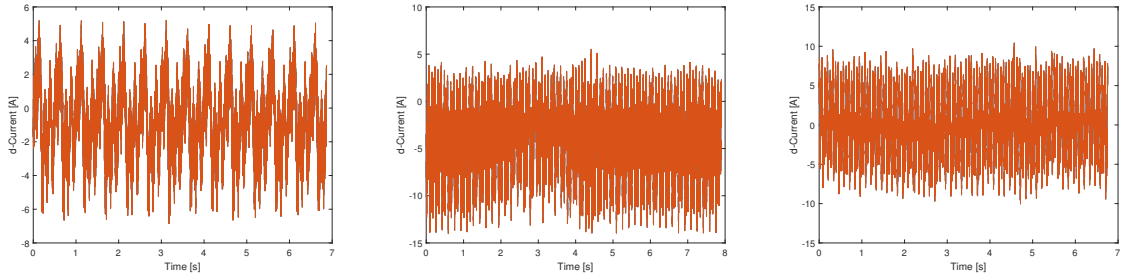

(a) 120 rpm *(b) 360 rpm* *(c) 480 rpm*

Figure 7: d-currents for one of the motor segments at various rotational speeds

7. Discussion

Using cascaded control loops in combination with a nine phase machine, an operational bearingless drive has been build that controls the rotors position in two dimensions as well as its rotational speed. Energy used for the bearing function is limited, but not insignificant. Further refinement of the control strategy should be investigated to try and reduce this effort. Also, the models that surved as the starting point for the controller design have been serious simplifications of reality. Extending the models to include coupling terms and non-linear effects of for example the rotor's position on electromagnetic properties could improve performance. Furthermore, the controller relies on highly precise, real-time measurements of the rotor's position. Sensors able to provide these signals in underwater conditions are costly. Hence, the possibility of replacing these sensors with an adequate observer is also a subject for further study.

8. Conclusion

All in all, a working prototype of a hub-less bearingless rim-driven thruster has been build and tested both in lab conditions and in the field. Results are promising and encourage further research and development steps. The 4kW machine has already been scaled up to 20kW, which can in the future be increased further. Both machines have been tested succesfully in a lab environment as well as in the field. Additional research will be conducted to further improve the bearing performance and reduce its energy consumption.

References

Ahad, M. A. & Ahmad, S. M. (2021), Investigation of a 2-dof active magnetic bearing actuator for unmanned underwater vehicle thruster application, *in* 'Actuators', Vol. 10, MDPI, p. 79.

Chen, J., Zhu, J. & Severson, E. L. (2019), 'Review of bearingless motor technology for significant power applications', *IEEE Transactions on Industry Applications* **56**(2), 1377–1388.

Sokolov, M. et al. (2021), 'Bearingless motors: Modeling and control'.

Wang, F., Zhu, Y., Wang, H. & Zhao, D. (2019), 'Design and analysis of a bearingless permanent-magnet motor for axial blood pump applications', *IEEE Access* **8**, 7622–7627.